On the Influence of Hard Walls on Structural Properties in Polymer Glass Simulation

Jörg Baschnagel* and Kurt Binder

Institut für Physik, Johannes-Gutenberg Universität, Staudinger Weg 7, D-55099 Mainz, Germany

Received April 12, 1995; Revised Manuscript Received July 6, 1995®

ABSTRACT: Structural properties of a dense polymer melt confined between two hard walls are investigated over a wide range of temperatures by dynamic Monte Carlo simulation using the bond-fluctuation lattice model. The temperatures studied vary between those of the ordinary liquid and those of the strongly supercooled melt. At high temperatures the configurational properties of the polymers close to the walls exhibit the following features: The density profiles of the monomers and of the end monomers are enhanced at the walls and decay toward the bulk value on the length scale of the bond. Both the bonds and the chains tend to align preferentially parallel to the wall. The radius of gyration is the largest length scale characterizing the extent of the interfacial region. When the melt is progressively supercooled, all features of the profiles and the tendency of parallel orientation with respect to the walls become more pronounced. For the strongly supercooled melt the perturbation introduced by the presence of the walls penetrates deeply into the bulk, decaying on a length scale which is larger than the radius of gyration.

I. Introduction

Many high-performance materials are polymer–matrix composite materials, in which a fibrous component (e.g., glass, Kevlar, graphite) is embedded in an amorphous polymer matrix (e.g., epoxies, polyesters, polyimides).[1,2] The advantage of combining a polymer system and a fiber is to design a new material with specifically tailored properties which none of the individual components possesses alone. The fiber component generally serves to reinforce the specific modulus and the specific strength of the (usually) mechanically weak polymer matrix, whereas the matrix determines the overall physico-chemical properties of the composite material (i.e., chemical resistance, thermal expansion etc.). Such fiber-reinforced polymer composite materials are lighter than the conventional ceramic or metallic materials while exhibiting comparable or even better thermal and mechanical properties. Therefore they have gained wide acceptance as substitutes for ceramics or metals and find growing application in the automotive, aerospace, and electronic industry.[3–6]

Despite the widespread technical importance of the polymer–matrix composite materials, their properties are not yet well understood theoretically. The properties of these materials are substantially determined by the interaction between the fiber and the polymer component at the interface. The *interface* and the adjacent interfacial region, the so-called *interphase*, are schematically depicted in Figure 1. This figure sketches a small section of a composite material, where a polymer melt is immersed between two long threads of the fiber component. Whereas the polymers in the middle (i.e., in the matrix) are unaffected by the presence of the fiber and exhibit typical bulk behavior (Gaussian coil structure,[7] etc.), the *structure and the mobility* of the chains in the interphase are strongly influenced by the specific interaction with the fiber component, by the internal properties of the polymers (flexibility, degree of branching, etc.) and by external control parameters such as temperature or density. Such an influence is not only apparent from direct experimental studies of the morphology in fiber-reinforced polymer composite materials[2] but is also expected from the numerous experimental,[8–12] simulation,[13–37] and analytical[38–47] investigations of polymer systems close to interfaces or surfaces.

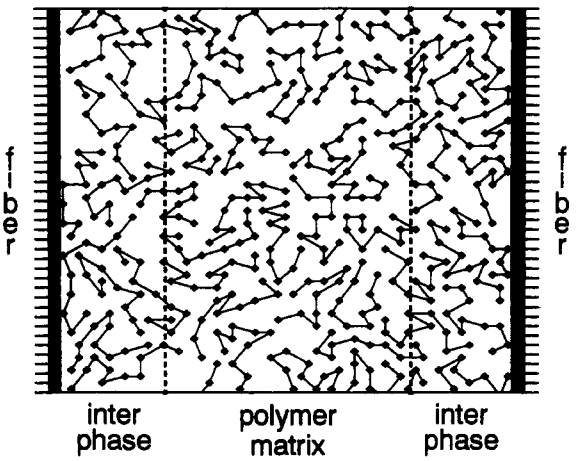

Figure 1. Schematic illustration of the interphase between a fiber component and an amorphous polymer matrix [after ref 2 (changed)]. The interaction between the fiber component and the polymer matrix (modeled by a pure hard core repulsion in this simulation) strongly influences the structure and the mobility of the polymer melt within the interphase, whereas the polymers sufficiently away from the interface in the matrix behave like chains in the unconstrained bulk.

In many of the cited simulations the solid–polymer melt interface is modeled by a hard neutral wall (i.e., no preferential attraction for the monomers occurs). The structure of the melt close to a hard wall is determined by two opposing factors: *packing constraints* and *loss in configurational entropy*. The loss in configurational entropy results from the reduction of accessible chain configurations due to the presence of the impenetrable wall. It produces an effective force which tries to drive the polymers away from the interface into the bulklike matrix. This effective force has to compete with another force (also entropic in origin) exerted by the chains in the matrix on the polymers at the interface, which tends to pack them against the wall. For long chain lengths and at low densities the entropic repulsion from the

* To whom correspondence should be addressed.

® Abstract published in *Advance ACS Abstracts,* August 15, 1995.

0024-9297/95/2228-6808$09.00/0

interface prevails and leads to a depletion of the region near the wall, whereas the packing constraints gradually counterbalance this repulsive force and start to dominate for short chains as the density increases. At meltlike densities the polymers in the matrix press the chains near the wall against the interface and force them to orient parallel to it to some extent. This influence on the structure of the polymers, resulting from the interplay of density and chain entropy, close to a hard wall has been observed in molecular dynamics simulations,[18] in off-lattice Monte Carlo simulations,[20,21,23,24,29-32,34,35,39-41] and in lattice Monte Carlo simulations[25-28,37] and can also be rationalized theoretically.[38-44,46]

The advantage of the mentioned simulations is that the structural (and dynamical) properties at the polymer–wall interface can be analyzed simultaneously on different length scales by suitably defined quantities. Among these quantities are, for instance, various profiles which characterize how the influence of the wall gradually vanishes with increasing distance from it, such as the monomer density profile, the chain density, profile, and the profile of the bond orientation or of the radius of gyration. Whereas most of the mentioned simulations study the variation of these profiles with chain length,[18,19,23,25-29,31,3237] density,[29-32,34,35,37] overall distance between the walls,[23,26,27,34,35] or a change in the wall potential (i.e., attractive potentials of variable strength),[18,25,36,28] not much work has been done on the variation of the profiles with temperature. With the present simulation we want to contribute solving to this problem by studying a confined polymer melt in a temperature interval that ranges from the ordinary liquid to the strongly supercooled state close to the glass transition of the bulk.

How confinement influences the glassy behavior of a substance is still rather controversial. There are experimental studies of the glass transition of organic liquids in small pores, which yield either a decrease or an increase of the glass transition temperature T_g with respect to the bulk. For instance, a reduction of T_g by the finite pore size was found in differential scanning calorimetry measurements of *o*-terphenyl and benzyl alcohol,[48] whereas an increase of T_g with confinement was reported in dielectric relaxation investigations of propylene glycol.[49] An increase of T_g was also observed in a recent molecular dynamics simulation of a binary mixture of soft spheres which are confined between two parallel plates.[50] On the other hand, ellipsometric studies of thin glassy polymeric films indicate that T_g decreases when the polymer interacts only weakly with the substrate, but increases when the interaction is strong.[51-53] In the former case the reduction of T_g with respect to the bulk is attributed to the formation of a liquidlike layer on the free surface of the film, where the mobility of the polymers is considerably enhanced.[51] In the latter case it is speculated that this layer also exists, but that its effect is outweighed by the interaction with the substrate.[52,53] In view of this rather controversial experimental situation it seems worthwhile to study the influence of confinement on the glass transition in a largely simplified (polymer) model for which much is known about the glassy behavior of the bulk.

The remainder of the paper is organized as follows: In section II we describe the model used in the simulation and some technical details of the simulation itself. The main part of the paper (section III) presents the results of the influence of temperature on the structural properties of the confined polymer melt. Section IV contains our conclusions and provides a brief outlook on future work.

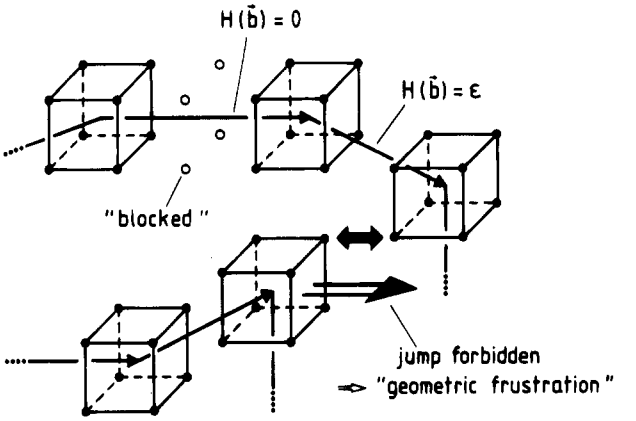

Figure 2. Sketch of a possible configuration of monomers belonging to different chains in the melt in order to illustrate the effect of $\mathcal{H}(\vec{b})$. All bond vectors shown in this picture have the energy ϵ except the vector (3,0,0) which belongs to the ground state. This vector blocks four lattice sites (marked by ○) which are no longer available to other monomers, since two monomers may not overlap. Due to this excluded volume interaction the jump in direction of the large arrow is also forbidden.

II. Model and Simulation Technique

The polymer melt is simulated by the bond-fluctuation model.[54] In this model the polymers are represented by self-avoiding and mutually avoiding walks on a simple cubic lattice and consist of monomers which occupy a whole unit cell of the lattice. Due to this identification of a monomer with a unit cell a multitude of bond vectors are a priori possible (in other lattice models, where a monomer is associated with a single lattice site, the number of bond vectors is essentially identical to the (small) coordination number of the lattice[55]). This multitude of bond vectors is reduced to a set of 108 allowed bond vectors by two conditions: local self-avoidance of the monomers and uncrossability of the bond vectors during the course of the simulation (no phanton chains[7]). The 108 allowed bond vectors are obtained from the set {(2,0,0), (2,1,0), (2,1,1), (2,2,1), (3,0,0), (3,1,0)} by all symmetry operations of the simple cubic lattice. Though finite, the number of available bonds is large enough to make the model approximate the continuous space behavior fairly well.[56,57] Whereas this applies for all quantities which extend over several lattice constants, the lattice structure has to leak through in the profiles to be studied. It is one of the purposes of this paper to find out which features of the profiles are introduced by the underlying lattice and which have been or might also be observed in corresponding continuous space simulations and real materials.

In addition to the excluded volume interaction an energy function $\mathcal{H}(\vec{b})$ is associated with each bond vector $\vec{b}$, which favors the bonds of length $b = 3$ and direction along the lattice axes (i.e., $\mathcal{H}(\vec{b}) = 0$) in comparison to all other available bond vectors (i.e., $\mathcal{H}(\vec{b}) = \epsilon$).[57,58] Figure 2 illustrates the effect of this energy function. When the temperature decreases, each bond tries to reach the ground state (i.e., a bond with $\mathcal{H}(\vec{b}) = 0$) and thereby blocks four lattice sites for other monomers. This loss of available volume generates a competition between the energetically driven expansion of a bond and the density of the melt. Due to this competition the melt exhibits no tendency to crystallize and may easily be supercooled. Various static and dynamic properties of the unconfined supercooled melt (i.e., of the pure bulk polymers unconfined by the walls) have been studied.[58,59] These simulations show that the present simple model reproduces many aspects of experimental

(polymeric) glass formers:[60,61] Structural relaxation functions become strongly stretched when the melt is progressively supercooled, and the corresponding relaxation times increase in a non-Arrhenius fashion.[58] If the melt is cooled at a finite rate, it falls out of equilibrium at low temperatures and freezes in an amorphous structure on the time scale of the simulation. The glass transition temperature depends on cooling rate and inverse chain length in a nonlinear and in a linear fashion, respectively.[58] If the melt is cooled quasistatically to temperatures as low as possible, the entropy per monomer continuously decreases and starts to level off for very low temperatures close to the glass transition (i.e., for $T < 0.2$[64]).[59] All of these results are borne out by experiments.[60,61]

Since the model has turned out to be well suited for the investigation of the glassy behavior of the bulk, it seems promising that it might also yield some insight in the static and dynamic properties of supercooled polymer melts in confined geometry. As a first step in this direction, we study in the present paper the change in the structure of a polymer melt confined between two hard walls (see Figure 1) when the temperature decreases from values typical of an ordinary liquid (i.e., $T = 1.0$) to those close to the glass transition temperature of the bulk (i.e., $T = 0.2$).[64] The lowest temperature $T = 0.2$ studied here corresponds to a strongly supercooled melt. The hard walls are inserted in the z direction at $z = 0$ and $z = H = 40$, whereas periodic boundary conditions are used in the x and y directions. The size of the simulation box in these directions is $L_x = L_y = L = 40$, which is large enough to ensure that a chain does not interact with its periodic images [i.e., $L > 2R_G^{bulk}$, where R_G^{bulk} is the radius of gyration of the chains in the bulk (i.e., in the matrix, see Figure 1)]. The simulation box contains $P = 390$ monodisperse polymer chains with a length of $N = 10$ monomers. Since each monomer occupies 8 lattice sites on the simple cubic lattice, the density of the melt is $\phi = 8NP/(H - 1)L^2 = 0.5$ (i.e., a volume fraction of 50% of the lattice sites is occupied). This density suffices to make the model exhibit the behavior typical of dense polymer melts.[62]

Ten of these simulation boxes are treated in parallel to gather statistics. However, preliminary test runs have shown that the statistical effort provided by these ten independent configurations is by far not sufficient to determine the various profiles with adequate accuracy. In order to improve the statistics independent configurations have to be generated during the simulation, which means that the waiting time between consecutive measurements must be of the order of the structural relaxation time.

With the usual bond-fluctuation dynamics this structural relaxation time increases strongly with falling temperature, as mentioned above, which would make the generation of statistically independent configurations prohibitively difficult in the interesting temperature region. The usual bond-fluctuation dynamics consists in moving a randomly chosen monomer in a random direction along the lattice axes. These *local* moves are supposed to mimic a random force exerted on a monomer by its environment. They lead to Rouse-like dynamics, which is typical of a polymer in a dense melt.[7] However, one of the advantages of the Monte Carlo technique is that the move may be adapted to the problem at hand. Since the equilibrium state is independent of the way by which it is reached, one need not necessarily work with the *realistic* dynamics of local moves, but may replace it by an *artificial* one which uses *global* moves to speed up the equilibration of the melt. A global move involves a collective motion of all monomers of a chain. Such a collective motion may be realized by the so-called *slithering snake dynamics*,[55,63] for instance. In the slithering snake dynamics one attempts to attach a randomly chosen bond vector (from the set of allowed bond vectors) to one of the ends of a polymer (both also randomly chosen). If the attempt does not violate the excluded volume restriction, the move is accepted with probability $\exp[-\Delta\mathcal{H}/k_BT]$, where $\Delta\mathcal{H}$ is the energy difference between the newly added bond and the last bond of the other end of the chain. This last bond is removed, provided the move is accepted. By means of the probability $\exp[-\Delta\mathcal{H}/k_BT]$ temperature is introduced in the simulation.[64]

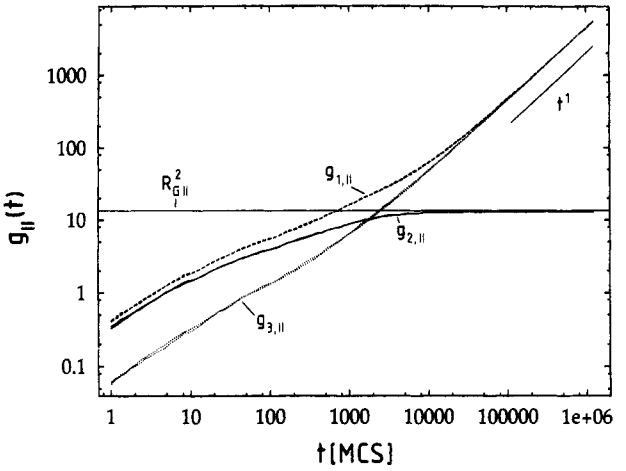

Figure 3. Time dependence of the parallel components of various mean square displacements (msd), i.e., of the monomers ($g_{1,II}(t)$, dashed line), of the monomers in the reference frame of the center of mass ($g_{2,II}(t)$, solid line), and of the center of mass ($g_{3,II}(t)$, dotted line) (see text for details). The data are generated by the slithering snake dynamics at the lowest temperature studied ($T = 0.2$). For each msd two curves are shown, one of which was obtained by using the end configuration of the first curve (i.e., the configuration after 1.25×10^6 MCS's) as the initial configuration. Since the curves for the different msd's coincide within the statistical accuracy, the slithering snake dynamics succeeds in equilibrating the melt at this temperature. In addition, two solid lines are shown: a horizontal one for the component of the radius of gyration parallel to the wall and one with slope 1 at late times.

Contrary to the usual Rouse dynamics the slithering snake dynamics does not slow down as drastically so that equilibration becomes possible down to $T < 0.2$. This has been demonstrated for the unconfined polymer melt in ref 65, and Figure 3 exemplifies this property of the slithering snake dynamics again for the confined melt. Figure 3 shows the time evolution of three mean square displacements, measured parallel to the wall, at $T = 0.2$, the lowest temperature of the present study: $g_{1,II}(t)$, the mean square displacement of the (two) inner monomers (exclusion of chain end effects); $g_{2,II}(t)$, the mean square displacement of the (two) inner monomers in the center-of-mass system and $g_{3,II}(t)$, the mean square displacement of the center of mass of the polymers. At early times the monomers do not feel the motion of the center of mass. Therefore $g_{1,II}(t)$ and $g_{2,II}(t)$ virtually start at the same value which is larger than that of $g_{3,II}(t)$ by a factor $1/N$. At late times the motion of the monomers has to follow that of the chain so that $g_{1,II}(t) \propto g_{3,II}(t) \propto t$ (for $t > 10^5$ MCS's) and $g_{2,II}(t)$ takes a constant value (i.e., the monomers do not move in the center-of-mass system). Due to this time dependence of the mean square displacements $g_{2,II}(t)$ and $g_{3,II}(t)$ must intersect. Since this intersection occurs at a time when $g_{3,II}$ has moved over a distance of about the radius of gyration (i.e., of its component parallel to the wall; see horizontal solid line in the figure), the time of the intersection may be identified with the structural relaxation time of a chain. Even at $T = 0.2$ the so-defined structural relaxation time is only about 2000 MCS's for the slithering snake dynamics, whereas the corresponding time for the usual bond-fluctuation dynamics is at least 3 orders of magnitude larger.[58] In the simulation the mean square displacements were also measured normal to the wall, yielding curves comparable to those of the parallel components except at long time (where the motion has to be confined by the presence of the walls). The final value of the structural relaxation time was then taken to be a value which exceeds the largest of the intersection times measured parallel and normal to the wall.

That this definition suffices to remove the history of the cooling process completely is illustrated in Figure 3 by the two curves which are shown for each mean square displacement. One of these curves corresponds to a simulation, where the start configuration was relaxed for the structural relaxation

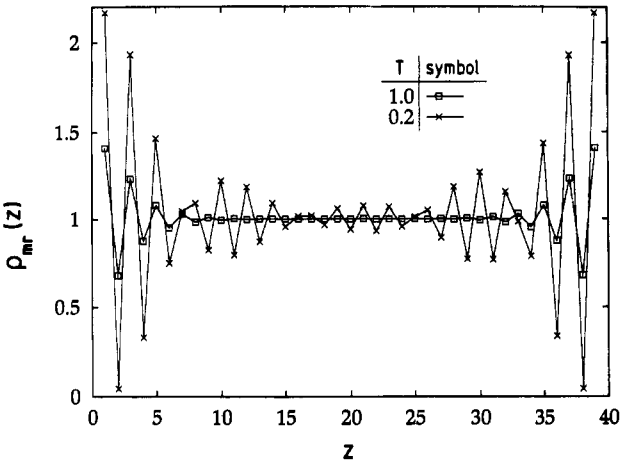

Figure 4. Plot of the reduced monomer density profile $\varrho_{mr}(z) = \varrho_m(z)/\varrho_m^{bulk}$ versus the distance z from the wall for $T = 0.2$ (×) and $T = 1.0$ (□). ϱ_m^{bulk} is the average of $\varrho_m(z)$ for $15 \le z \le 25$.

time defined above, whereas the start configuration for the other curve is the end configuration of the first curve. The two curves coincide within the statistical accuracy. There is sign of residual aging effects. Therefore the structural relaxation time defined above is a sufficient waiting time to obtain statistically independent configurations. In this way, 2000 additional configurations were generated for the further analysis. Since 10 independent configurations are simulated in parallel, the total statistical effort involves 20 000 configurations for each temperature. Therefore the statistical inaccuracy should be well under control in the present simulation.

III. Structural Properties of the Polymer Film

In order to study the competition between temperature, packing constraints, and wall effects on the structural properties of the polymer melt, distance profiles measured in the z direction normal to the (lower) hard wall were recorded during the simulation for various quantities which are sensitive to changes on different length scales of the melt. These length scales are the length scale of a monomer (i.e., of a lattice constant), of a bond, and of a chain. The subsequent sections report the results of this analysis.

A. Monomer Density Profiles. Figure 4 compares the dependence of the reduced monomer density profile $\varrho_{mr}(z)$ on z for the temperatures $T = 0.2$ (supercooled melt) and $T = 1.0$ (polymer melt at high temperature). The reduced monomer density profile is defined by $\varrho_{mr}(z) = \varrho_m(z)/\varrho_m^{bulk}$, where $\varrho_m(z)$ is the monomer density (i.e., the average number of monomers divided by L^2) at z and ϱ_m^{bulk} is the value of the profile in the matrix. A monomer is associated with the value z if the lower face of its unit cell belongs to the zth plane of the cubic lattice, and ϱ_m^{bulk} is calculated as the average of $\varrho_m(z)$ for $15 \le z \le 25$. The choice of this interval for the calculation of the bulk properties seemed appropriate, since the enclosed z values are separated by more than twice the bulk value of the radius of gyration (see Table 1) from the walls at both temperatures.

At both temperatures the monomer density profile exhibits a strongly oscillating structure which may be rationalized as follows: Chains close to an impenetrable wall lose configurational entropy, which favors a depletion of the region near the wall. On the other hand, they also experience an effective average force by the collisions with the chains further away from the interface, which tends to pack them against the wall. At high enough densities (i.e., meltlike densities) the packing constraints dominate over the loss in configurational entropy and cause the enhancement of the monomer concentration next to the wall (i.e., at $z = 1$, 39 in Figure 4) over the bulk value. The enhancement next to the wall leads to a reduction of the monomer density in the following layer (i.e., $z = 2$, 38) due to the excluded volume interaction, which in turn allows for another enhancement in the subsequent layer. This sequence of enhanced and reduced monomer densities continues over a few lattice constants, until the bulk value is recovered (at least for the larger temperatures; see discussion below), and is comparable to that of the pair-correlation function in both appearance and interpretation. Qualitatively similar fluid-like oscillations of the monomer density are observed in molecular dynamics[18] and off-lattice Monte Carlo simulations[21,23,24,32,34,35,40-42] and may also be understood analytically.[39-44] Of course, the quantitative details (such as the weight of the first peak, etc.) are different for the various models. We expect that our model provides qualitatively reliable information on all length scales larger than the lattice spacing.

Figure 4 shows that the intensity of the density oscillations close to the wall strongly increases with decreasing temperature. At $T = 0.2$ about twice as many monomers as at $T = 1.0$ populate the layer next to the wall. This strong increase may be explained by the action of the model's energy function. When the temperature decreases, the energy function makes the bond vectors adopt the ground state. Since a bond vector in the ground state (i.e., in the state {(3,0,0)}) is oriented along the lattice axes, such an orientation should be facilitated by the presence of the wall and thus the packing of the monomers should become more efficient. Therefore one expects not only the number of bonds in the ground state to increase next to the wall but also the number of monomers. A similar argument was presented in a recent off-lattice simulation of a

Table 1. Bulk Values of the Various Profiles Discussed in the Text[a]

T	$10^2\varrho_m^{bulk}$	N_{cm}^{bulk}	$10^3\varrho_c^{bulk}$	$\langle\mathcal{R}\rangle^{bulk}$	$b_\parallel^2 = 2b_\perp^2$	θ^{bulk}	$R_{G\parallel}^2 = 2R_{G\perp}^2$	$R_\parallel^2 = 2R_\perp^2$
0.20	6.006	2.556	6.050	0.126	5.790	109.78	13.51	78.71
0.25	6.037	2.209	6.054	0.288	5.558	105.39	12.06	69.40
0.30	6.069	2.019	6.081	0.448	5.334	102.08	11.02	62.99
0.35	6.104	1.917	6.104	0.573	5.162	100.27	10.43	59.45
0.40	6.122	1.858	6.121	0.662	5.039	99.29	10.06	57.35
0.50	6.144	1.797	6.143	0.768	4.895	98.44	9.69	55.19
0.60	6.156	1.768	6.158	0.824	4.817	98.12	9.51	54.21
0.70	6.162	1.753	6.163	0.857	4.774	97.93	9.41	53.62
0.80	6.169	1.743	6.167	0.878	4.746	97.84	9.35	53.26
0.90	6.171	1.737	6.171	0.892	4.727	97.79	9.31	53.10
1.00	6.172	1.731	6.172	0.903	4.710	97.76	9.27	52.84

[a] The bulk values are defined as the average of the respective profiles for $15 \le z \le 25$ at all temperatures.

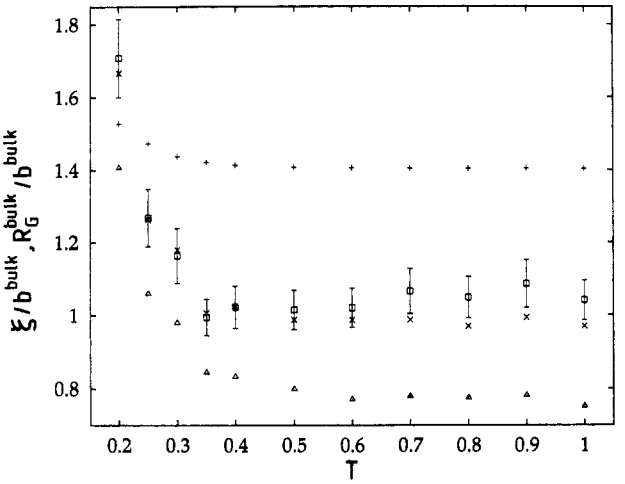

Figure 5. Temperature dependence of the decay length of the monomer density profile ζ_m (□), of the end-monomer density profile ζ_{em} (×), and of the chain-monomer profile ζ_{cm} (△). Additionally, the bulk value of the radius of gyration $R_G^{bulk} = (R_{G\parallel}^2 + R_{G\perp}^2)^{1/2}$ (+) is shown for comparison. R_G^{bulk} is the average of $R_G(z)$ for $15 \le z \le 25$. All quantities are normalized by the bulk bond length b^{bulk} defined in the same way as R_G^{bulk}. Note that R_G^{bulk}/b^{bulk} increases with decreasing temperature, which means that the chains stiffen.

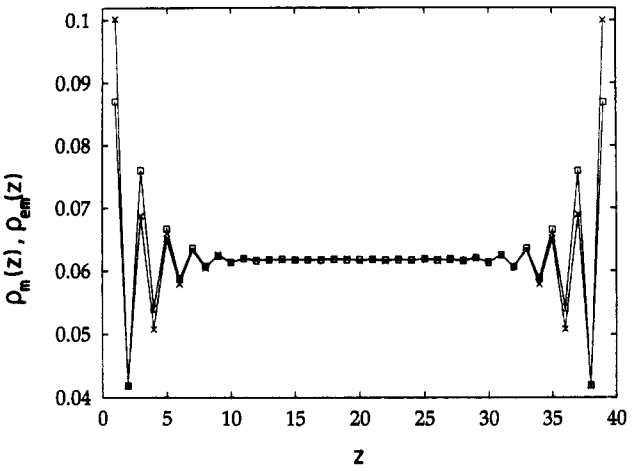

Figure 6. Comparison of the z dependence of monomer density profile $\varrho_m(z)$ (□) and the end-monomer density profile $\varrho_{em}(z)$ (×) at $T = 1.0$.

semiflexible polymer melt[34] and of a mixture of flexible and semiflexible polymers[41] to rationalize the further enhancement of the monomer density next to the wall when the chain stiffness was increased (over a certain range). Chain stiffness also increases in the present model with falling temperatures because of the interplay between the energy function and the density of the melt[58,65] (compare also the bulk values of the bond length and of the end-to-end distance, which are compiled in Table 1, and Figure 5). Therefore the findings of the cited off-lattice simulations suggest that the observed enhancement can result from the interplay between packing constraints and chain stiffness and is not a consequence of the underlying lattice structure.

The combined effect of the enhanced monomer density at the wall and the excluded volume interaction makes the intensity of the density oscillations increase and thus the monomer density profile decay more slowly toward the bulk value. Since the corresponding decay length may be used as a measure for the size of the interphase, its temperature dependence is of great interest. In order to quantify this temperature dependence one could try to read off the z value at which $\varrho_{mr}(z)$ attains the bulk value. Whereas this is possible for $T \ge 0.25$, the irregular structure of $\varrho_{mr}(z)$ hampers such an analysis at $T = 0.2$ (see Figure 4). Therefore a different approach is needed to estimate the size of the interphase at all temperatures. One way of doing this is as follows: The density profiles are symmetric around the middle of the simulation box. Therefore both halves may be combined to an average profile $\bar{\varrho}_m(z)$. This average profile can be used to define a probability for finding a monomer at position z by

$$p_m(z) = \frac{|\bar{\varrho}_m(z) - \varrho_m^{bulk}|}{\sum_{z=1}^{L/2} |\bar{\varrho}_m(z) - \varrho_m^{bulk}|} \qquad (1)$$

the first moment of which is a suitable quantity to characterize the decay of the monomer density profile, i.e.,

$$\zeta_m = \sum_{z=1}^{L/2} z p_m(z) \qquad (2)$$

In Figure 5 the temperature dependence of the ratio ζ_m/b^{bulk} is compared with that of R_G^{bulk}/b^{bulk}, where both the bulk radius of gyration and the bulk bond length are defined by $R_G^{bulk} = (R_{G\parallel}^2 + R_{G\perp}^2)^{1/2}$ and $b^{bulk} = (b_\parallel^2 + b_\perp^2)^{1/2}$ from the data compiled in Table 1. These definitions are legitimate, since the resulting value agrees with that from a simulation of the unconfined melt.[65] Figure 5 shows that ζ_m depends only weakly on temperature for $T \ge 0.35$, but increases by about a factor of 2 in the temperature region where the glassy behavior of the model starts to develop. This increase is much stronger than that of R_G^{bulk} in the same temperature range. For $T \ge 0.35$ the values of ζ_m are comparable to those of mean bond length in the bulk and thus much smaller than R_G^{bulk}. In the state of the ordinary liquid the radius of gyration is the relevant (large) length scale, whereas wall-induced longer ranged correlations develop in the supercooled confined melt. Close to T_g the subtle interplay of energy, density, and wall constraints seems to generate an additional length scale ζ_m which determines the size of the interphase. At $T = 0.2$ this length scale becomes large and incommensurable to the lattice constant and thus destroys for $z > \zeta_m$ the regular structure of $\varrho_m(z)$ (maxima at odd and minima at even values of z), which was present as long as $\zeta_m < R_G^{bulk}$ (i.e., as long as $T \ge 0.25$).

In addition to R_G^{bulk} and to ζ_m Figure 5 also includes the temperature dependence of ζ_{em}, the decay length of the end-monomer density profile $\varrho_{em}(z)$, which is defined analogously to ζ_m (see eq 2). The close agreement of the temperature dependences of ζ_{em} and ζ_m suggests that the corresponding profiles are also rather similar. The original profiles $\varrho_{em}(z)$ are defined as the average density of end monomers at position z multiplied by $N/2$ so that its bulk value (i.e., the value for $15 \le z \le 25$) coincides with ϱ_m^{bulk}. These profiles are compared with those of $\varrho_m(z)$ at $T = 1.0$ and $T = 0.2$ in Figures 6 and 7, respectively. Figure 6 shows that $\varrho_{em}(z)$ is larger than $\varrho_m(z)$ at the wall. An enhancement of the chain end density at the wall was also observed in molecular dynamics,[18] off-lattice Monte Carlo[23,24,34,35,39,40,44] and

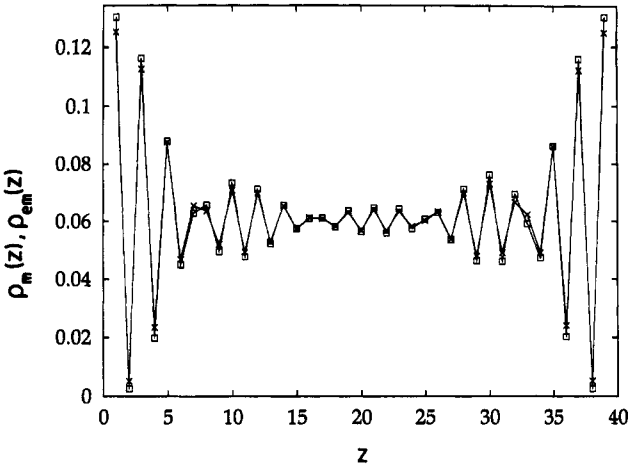

Figure 7. Comparison of the z dependence of monomer density profile $\varrho_m(z)$ (□) and the end-monomer density profile $\varrho_{em}(z)$ (×) at $T = 0.2$.

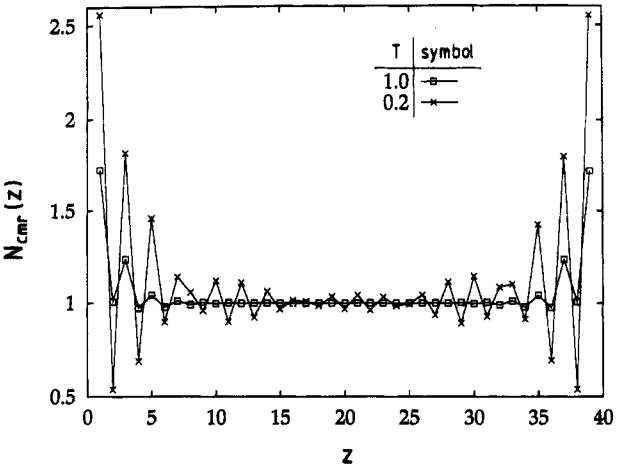

Figure 8. Plot of the reduced chain-monomer profile $N_{cmr}(z) = N_{cm}(z)/N_{cm}^{bulk}$ versus the distance z between the walls for $T = 0.2$ (×) and $T = 1.0$ (□). $N_{cm}(z)$ is the average number of monomers at position z, which belong to the same chain. ϱ_{cm}^{bulk} is the average of $\varrho_{cm}(z)$ for $15 \le z \le 25$.

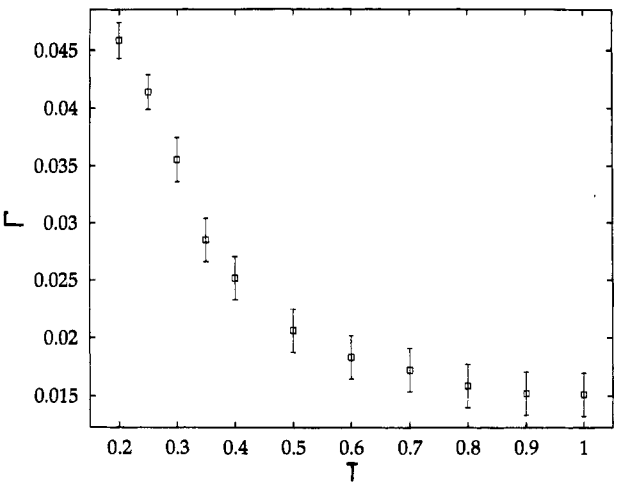

Figure 9. Temperature dependence of the adsorbed excess Γ defined by eq 3.

lattice Monte Carlo simulations[26-28] and can be rationalized as follows:[47] The presence of the impenetrable wall excludes a larger number of chain configurations with internal monomers touching the wall than of configurations with end monomers touching it. Therefore the enhancement of chain ends at high temperatures results from the attempt of the chains to minimize the loss in configurational entropy. With decreasing temperature the contribution of the energy function becomes important. As discussed with respect to Figure 4 the combined effect of the energy function and the hard wall is to align bonds in the ground state parallel to the wall. Therefore one can expect $\varrho_m(z)$ to increase strongly and eventually to become larger than $\varrho_{em}(z)$ at $z = 1$. Figure 7 shows that $\varrho_m(1)$ is indeed larger than $\varrho_{em}(1)$ at $T = 0.2$. A comparable inversion of $\varrho_m(1)$ and $\varrho_{em}(1)$ is not observed in off-lattice simulations of semiflexible polymer melts[34,40] with increasing chain stiffness, which suggests that the behavior of the monomer and end-monomer profile at the wall is particularly determined by the model and the conditions used in the simulation. In addition, Figures 5–7 reveal that the influence of the wall on $\varrho_{em}(z)$ vanishes on the *same* length scale as that on $\varrho_m(z)$. The evidence in favor of this observation from other simulations is not unambiguous. Whereas molecular dynamics simulations[18] and off-lattice Monte Carlo simulations[34,35,40] suggest that $\varrho_m(z)$ and $\varrho_{em}(z)$ decay on the same length scale (i.e., on that of the monomer diameter), other off-lattice Monte Carlo simulations[21,23,24,39] rather find that $\varrho_m(z)$ reaches the bulk value faster than $\varrho_{em}(z)$ which decays on the length scale of R_G^{bulk}. Therefore it seems that the appropriate decay length of $\varrho_{em}(z)$ depends on the model, the specific interactions, and the values of the external control parameters (i.e., temperature and density) employed in the simulation.

Another quantity which provides information on the structure of the polymers close to the wall is the chain-monomer profile. The chain-monomer profile $N_{cm}(z)$ proposed by Theodorou in ref 46 is defined as the average number of monomers in layer z that belong to the same chain. Figure 8 compares the z dependence of the reduced chain-monomer profile $N_{cmr}(z) = N_{cm}(z)/N_{cm}^{bulk}$ (N_{cm}^{bulk} is the average of $N_{cm}(z)$ for $15 \le z \le 25$; see Table 1) at $T = 0.2$ and $T = 1.0$. At both temperatures the characteristics of $N_{cmr}(z)$ are very similar to those of $\varrho_m(z)$ or $\varrho_{em}(z)$: The competition between wall effects and excluded volume interaction leads to oscillations in $N_{cmr}(z)$. The intensity of these oscillations increases with decreasing temperature, their decay toward the bulk value occurs on a length scale whose temperature dependence is qualitatively compatible with that of $\varrho_m(z)$ or of $\varrho_{em}(z)$ (see Figure 5), their regular structure is interrupted for $z > \zeta_m$, and their start value at the wall is enhanced over the bulk value. At $T = 1.0$ this start value is $N_{cm}(1) \approx 3$, whereas $N_{cm}(1) \approx 6.5$ at $T = 0.2$; i.e., six to seven monomers of the average number of monomers at the wall belong to the same chain at $T = 0.2$. This is an indication that not only the bonds but also the polymers tend to align parallel to the wall at low temperatures. Further evidence for this flattening of the chains will be given in the subsequent sections.

Another interesting quantity related to $\varrho_m(z)$ is the so-called adsorbed excess, defined by

$$\Gamma = \sum_{z=1}^{L/2} (\bar{\varrho}_m(z) - \varrho_m^{bulk}) \qquad (3)$$

which measures the amount of monomer in the interfacial region in excess of ϱ_m^{bulk}. The temperature dependence of Γ is depicted in Figure 9. The figure shows that the adsorbed excess is a small, but positive,

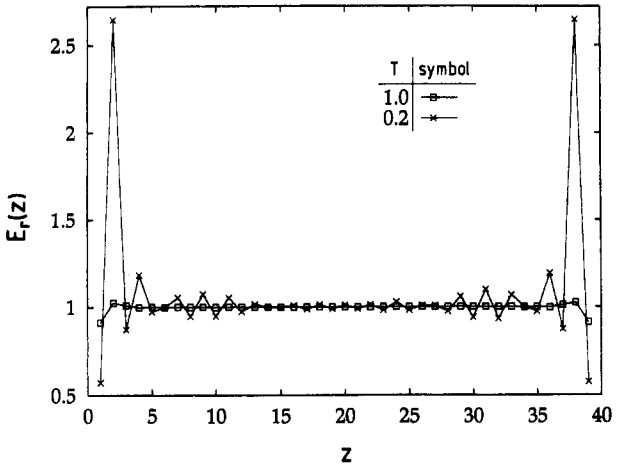

Figure 10. Plot of the reduced bond energy profile $E_r(z) = \langle\mathcal{H}\rangle(z)/\langle\mathcal{H}\rangle^{bulk}$ versus z for $T = 0.2$ (×) and $T = 1.0$ (□). $\langle\mathcal{H}\rangle^{bulk}$ is the average of $\langle\mathcal{H}\rangle(z)$ for $15 \le z \le 25$. The z value of $E_r(z)$ is defined to be the z position of the monomer from which the bond starts.

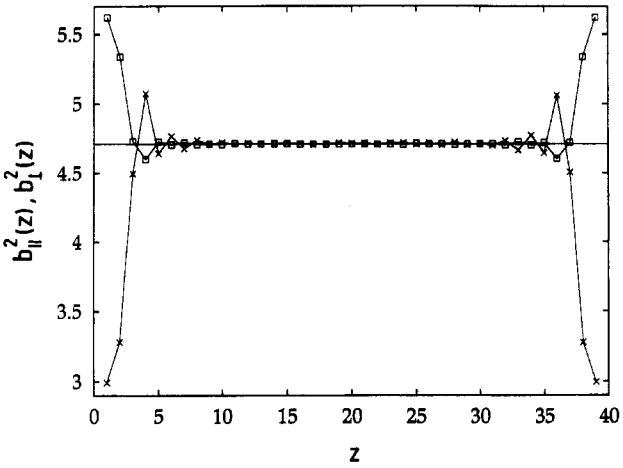

Figure 11. Plot of the distance profiles of the component of the mean square bond length parallel $[b_{||}^2(z) = b_x^2(z) + b_y^2(z)$; □] and perpendicular $[2b_\perp^2(z)$; ×] to the wall at $T = 1.0$. The z value of the profiles is defined to be the z position of the monomer from which the bond starts. The horizontal solid line is the bulk value from Table 1.

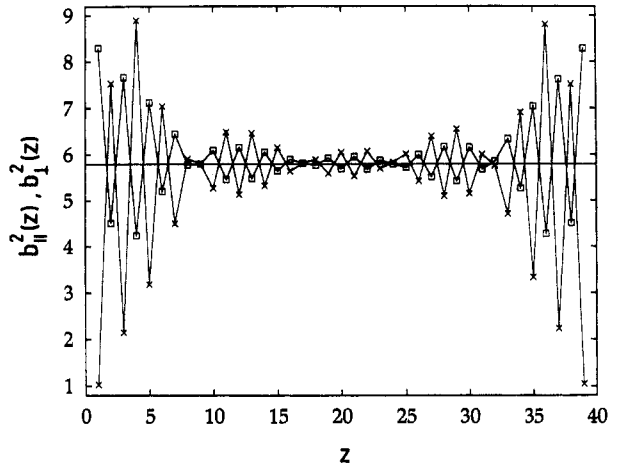

Figure 12. Plot of the distance profiles of the component of the mean square bond length parallel $[b_{||}^2(z)$; □] and perpendicular $[b_\perp^2(z)$; ×] to the wall at $T = 0.2$. The z value of the profiles is defined to be the z position of the monomer from which the bond starts. The horizontal solid line is the bulk value from Table 1.

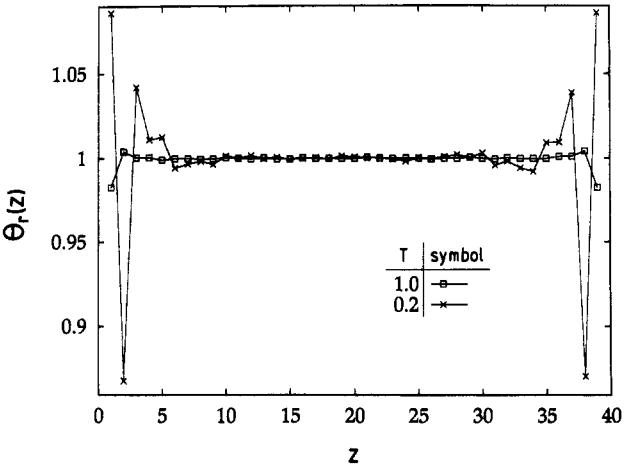

Figure 13. Plot of the reduced bond angle profile $\Theta_r(z) = \Theta(z)/\Theta^{bulk}$ versus z for $T = 0.2$ (×) and $T = 1.0$ (□). Θ^{bulk} is the average of $\Theta(z)$ for $15 \le z \le 25$. The z value of $\Theta_r(z)$ is taken to be the z position of the monomer joining the two bonds which define the angle.

quantity which increases by about a factor of 3 in the studied temperature interval. This illustrates again the fact that—although there is no attraction between the monomers and the walls—the dominance of the packing constraints leads to an effective force which presses the chains against the wall and which becomes enhanced by the contribution of the model's energy function. This behavior of the adsorbed excess is to be expected, since our model has a negative thermal expansion (i.e., as the temperature decreases, the chains expand by occupying a larger volume[59]) and since the energetic preference of $\vec{b} = \{3,0,0\}$ is compatible with bonds lying parallel to the wall at low temperatures.

B. Profiles on the Length Scale of a Bond. In order to study the structural properties of the confined polymer melt on the length scale of a bond, Figures 10–13 present the reduced profile of the mean energy per bond (i.e., $E_r(z) = \langle\mathcal{H}\rangle(z)/\langle\mathcal{H}\rangle^{bulk}$), the profiles of the mean square bond length parallel $b_{||}^2(z)$ and perpendicular $2b_\perp^2(z)$ to the wall, and the reduced profile of the mean bond angle (i.e., $\Theta_r(z) = \Theta(z)/\Theta^{bulk}$). The profile of $2b_\perp^2(z)$ is multiplied by 2 in order to make its value in the bulk coincide with that of $b_{||}^2(z) = b_x^2(z) + b_y^2(z)$. The z values of the profiles for the mean energy per bond and for mean square bond length are taken to be the position of the monomer from which the bond emanates, and those of the profile for the mean bond angle are associated with the position of the middle monomer joining the two bonds which define the angle.

The mean energy per bond varies between 0 and 1 by definition and can thus be considered as a measure for the probability to find a bond vector in the excited state (i.e., in the state $\mathcal{H}(\vec{b}) = \epsilon^{64}$). Table 1 shows that at $T = 1.0$ 90% of the bond vectors in the bulk are in the excited state, whereas this percentage reduces to about 13% at $T = 0.2$. This reduction becomes even more pronounced in the immediate vicinity of the wall (see Figure 10). At $T = 1.0$ and $T = 0.2$ the percentage of bonds in the excited state at $z = 1$, 39 is about 82% and about 7%, respectively. In other words, about 93% of the bond vectors are in the ground state at $T = 0.2$, the vast majority of which are oriented parallel to the wall. This becomes apparent from the profiles of the mean square bond length (see Figures 11 and 12). First of all, these profiles show that the impenetrable wall favors a parallel alignment quite generally at all temperatures. This influence of the wall on the orientation of the bond vectors was also observed in other simula-

tions[18,19,21,23,24,26,34] and predicted theoretically.[46] However, at $T = 0.2$ $b_{||}^2(z)$ is strongly enhanced over its value at $T = 1.0$ and is rather close to the low-temperature limit (i.e., $b_{||}^2(z) = 9$), whereas $2b_{\perp}^2(z)$ is almost negligible at the wall. That most of the bond vectors in the ground state lie parallel to the wall at $T = 0.2$ can also be inferred from the profile of the mean bond angle (see Figure 13). The bond angle between two successive bond vectors in the ground state is either 90° or 180°. In a layer there are two possibilities to realize the 90° and one to realize the 180° angle. If one ignores the influence of density completely, one can estimate the mean bond angle to be $\Theta \approx 2 \times 90°/3 + 180°/3 = 120°$. But this is exactly the number which results from Figure 13 and from the bulk values of Table 1. In summary, all of these profiles show that the model's energy function strongly reinforces the alignment constraints imposed on the polymers at the interface by the hard wall.

In the layers further away from the wall the various bond profiles reflect that there is a considerable difference in the structure of the melt at high and at low temperatures. At $T = 1.0$ both $E_r(z)$ and $\Theta_r(z)$ differ only slightly for $z > 1$ from their respective bulk values. The bulk values are reached for $z \approx 4$, i.e., for a z value comparable to $2b^{bulk} = 2(b_{||}^2 + b_{\perp}^2)^{1/2}$ (see Table 1). This is also the length scale on which $b_{||}^2(z)$ and $2b_{\perp}^2(z)$ start to fluctuate around the bulk value, as Figure 11 shows. However, for smaller z values the profiles of mean bond length components deviate more strongly from the result in the bulk than those of the bond energy or bond angle. For $z = 2$ $b_{||}^2(z)$ is still larger than $2b_{\perp}^2(z)$, whereas the situation is exactly reversed for $z = 4$. It is unlikely that the large component parallel to the wall at $z = 2$ results from parallely oriented bond vectors, as was the case for $z = 1$, since the monomer density and the chain-monomer profile show that the overall number of monomers at $z = 2$ is smaller than in the bulk and that on average only one to two of these monomers belong to the same chain. Therefore the large $b_{||}^2(2)$ value should be attributed to bond vectors such as {(2,1,0), (2,1,1), (2,2,1), (3,1,0)}, which can connect monomers from the enriched layers at $z = 1, 3$ to those at $z = 2$ with a large parallel component. Contrary to that, the large $2b_{\perp}^2(z)$ values at $z = 4$ may be rationalized by the contribution of the vectors (0,0,−3), (±1,0,−3), and (0,±1,−3) to $2b_{\perp}^2(z)$, which are excluded by the hard wall for smaller z values.

When the temperature decreases, the rather smooth z dependence of all profiles at $T = 1.0$ vanishes and a more or less pronounced oscillatory structure develops. Remembering the monomer density profiles, one can interpret this oscillatory structure in the following way: Figures 4 and 8 show that the overall number of monomers and number of monomers belonging to the same chain are strongly increased for $z = 1$, 3, 5 and strongly decreased for $z = 2$, 4 at $T = 0.2$. This regularly oscillating structure of both monomer profiles is interrupted for $z \geq 7$, i.e., for $z > \zeta_m$. Similar features are found for the various bond profiles. The maxima (minima) in the monomer profiles correspond to maxima (minima) in $b_{||}^2(z)$ and $\Theta_r(z)$ and to minima (maxima) in $E_r(z)$ and $2b_{\perp}^2(z)$ for $z \leq 5$. This means that the layers with an enhanced number of monomers also contain an enhanced number of bonds in the ground state, which are aligned parallel to the wall, whereas the bonds in the depleted layers are preferentially in the excited state and oriented perpendicular to the wall. This comparison of the various profiles suggests that the interplay of energy, excluded volume, and wall effects makes large portions of the polymers adopt entropically unfavorable flat configurations in the close vicinity of the wall and that this deviation from the isotropic chain configuration also perturbs the structural properties of the polymers in the bulk.

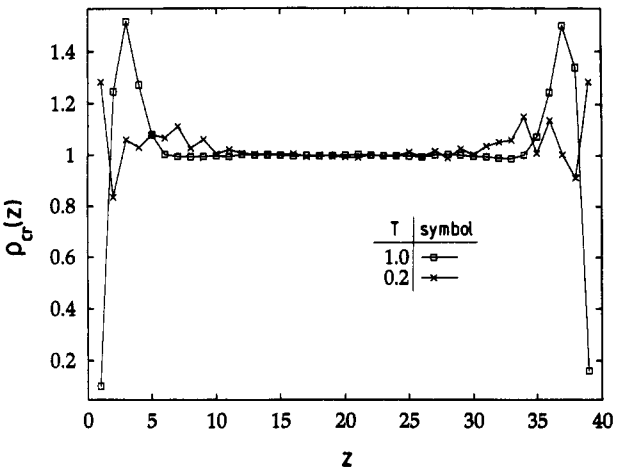

Figure 14. Plot of the reduced chain density profile $\varrho_{cr}(z) = \varrho_c(z)/\varrho_c^{bulk}$ versus z for $T = 0.2$ (×) and $T = 1.0$ (□). ϱ_c^{bulk} is the average of $\varrho_c(z)$ for $15 \leq z \leq 25$. The z value of $\varrho_{cr}(z)$ is taken to be that of the center of mass of the polymer.

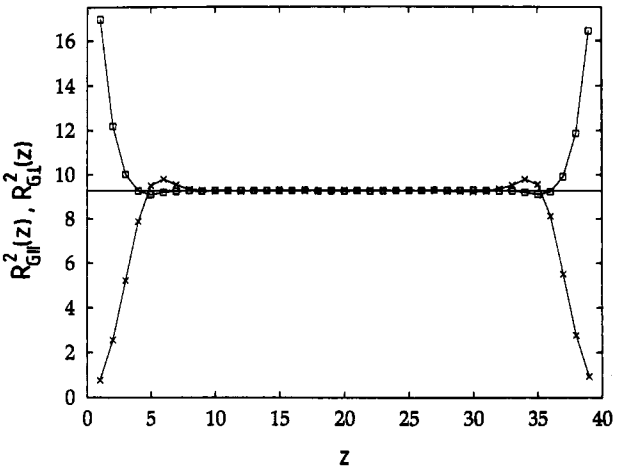

Figure 15. Plot of the distance profiles of the component of the radius of gyration parallel $[R_{G||}^2(z) = R_{G,x}^2(z) + R_{G,y}^2(z)$; □] and perpendicular $[R_{G\perp}^2(z)$; ×] to the wall at $T = 1.0$. The z value of the profiles is that of the center of mass of the polymer. The horizontal solid line is the bulk value from Table 1.

C. Profiles on the Length Scale of a Chain. This section deals with the structural properties of the confined polymer melt on the length scale of a chain. The influence of the hard wall constraint on the shape of the polymers is exemplified by the reduced chain density profile (i.e., $\varrho_{cr}(z) = \varrho_c(z)/\varrho_c^{bulk}$; see Figure 14) and by the profiles of the radius of gyration parallel $R_{G||}^2(z)$ and perpendicular $2R_{G\perp}^2(z)$ to the wall (see Figures 15 and 16). As for the profile of the mean square bond length $R_{G\perp}^2(z)$ is multiplied by a factor of 2 to make its value coincide with that of parallel component $R_{G||}^2(z) = R_{G,x}^2(z) + R_{G,y}^2(z)$ when the chain configuration is isotropic. The z values of all profiles in this section are taken to be the position of the center of mass of the polymers, and the center of mass is associated with position z if it lies in the interval $[z - 0.5, z + 0.5]$.

From the comparison of Figures 14 and 15 the following conclusions may be drawn about the structure

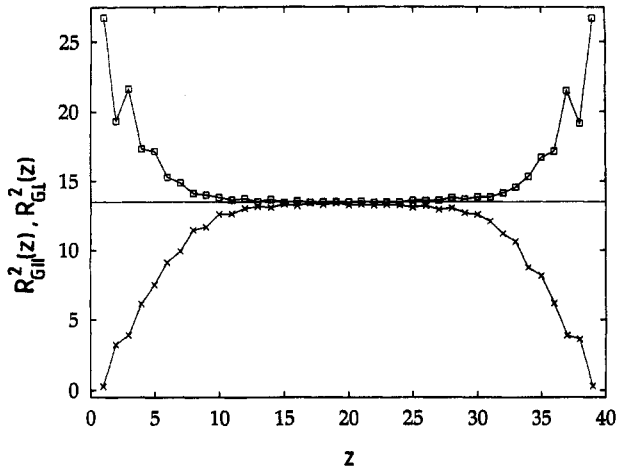

Figure 16. Plot of the distance profiles of the component of the radius of gyration parallel [$R_{G\parallel}^2(z)$; □] and perpendicular [$R_{G\perp}^2(z)$; ×] to the wall at $T = 0.2$. The z value of the profiles is that of the center of mass of the polymer. The horizontal solid line is the bulk value from Table 1.

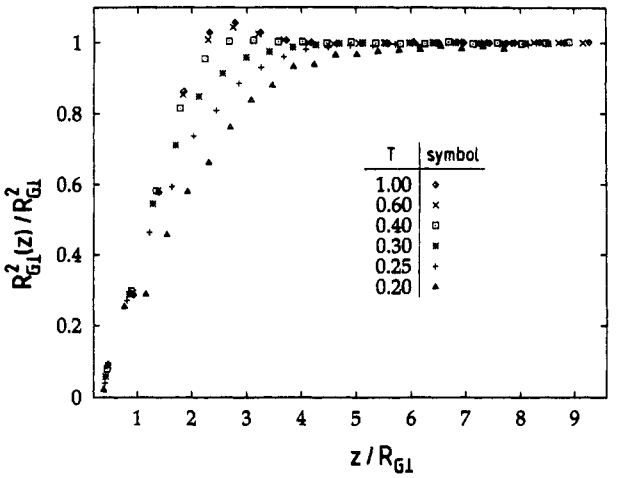

Figure 17. Plot of $R_{G\perp}^2(z)/(R_{G\perp}^{bulk})^2$ versus $z/R_{G\perp}^{bulk}$ for various representative temperatures: $T = 1.0$ (◇), $T = 0.6$ (×), $T = 0.4$ (□), $T = 0.3$ (*), and $T = 0.2$ (△). The z value of the profiles is that of the center of mass of the polymer.

of the melt at $T = 1.0$: Since $R_{G\parallel}^2(z) = 2R_{G\perp}^2(z)$ for $15 \leq z \leq 25$, the "soap-shaped" polymers can adopt all possible orientations and thus appear spherically isotropic in the bulklike inner part of the simulation box. The presence of the wall starts to be felt at $z \approx 8 \approx 2R_G^{bulk}$ (see Table 1). As the wall is further approached, the ability of the chains to reorient is progressively hindered, leading to an increase of $R_{G\parallel}^2$ and to a decrease of $R_{G\perp}^2$. Therefore the main effect of the wall is to reduce the orientational entropy of the polymers and to align them preferentially parallel to it. Only the few chains lying in the layer immediately adjacent to the wall are somewhat distorted and flattened. This influence of the wall on the chain structure is expected from the discussion of the profiles presented in the previous sections and is also confirmed by other simulations.[18,21,23-28,31,33-37,39,40]

When the temperature decreases, the contribution of the model's energy function reinforces the tendency of the chains to align parallel to the wall. This conclusion drawn from the discussion of the previous section is also corroborated by Figures 14 and 16. Contrary to $T = 1.0$ the layer at the wall is no longer depleted of, but enriched by, chains. These chains are much more flattened than those at high temperatures. The pronounced increase of chains at $z = 1$ induces a depletion of the subsequent layer, which in turn allows for another (smaller) enhancement of chains at $z = 3$. Therefore the interplay between energetic, packing, and wall constraints leads to a layering of the polymers, which is reflected by the zigzag structure of $R_{G\parallel}^2(z)$ close to the wall. The maxima of $R_{G\parallel}^2(z)$ coincide with those of the chain-monomer profile $\varrho_{cr}(z)$ for $z \leq 5$. As soon as the regular sequence of maxima and minima of $\varrho_{cr}(z)$ becomes interrupted (i.e., for $z > 7$; see Figure 8), the profiles of the radius of gyration begin to smooth. Therefore the regular oscillatory structure present to a varying extent in all profiles discussed so far at low temperatures must be attributed to the layering of the polymers in the proximity of the wall. This entropically unfavorable configuration gradually starts to cross over to the isotropic bulklike structure for $z \approx R_G^{bulk} - 2R_G^{bulk}$ for $\varrho_{cr}(z)$, $R_{G\parallel}^2(z)$, and $2R_{G\perp}^2(z)$. However, the profiles reach the bulk value only for $15 \leq z \leq 25$ and thus for z values which are larger than $2R_G^{bulk}$ (see Table 1).

This observation from Figures 14 and 16 indicates again (see discussion of Figure 5 for comparison) that R_G^{bulk} is not the relevant large length scale for the low-temperature properties of the confined melt. If it was the relevant length scale, one should be able to make the various chain profiles collapse onto a master curve when the ordinate and the abcissa values are divided by suitable powers of $R_{G\perp} = R_G^{bulk}/\sqrt{3}$. Since such a scaling merely corresponds to a change of the ordinate and abcissa values without affecting the shape of the profiles, it can only be expected to work if the structures of the curves are similar to each other. This is the case at high temperatures. That the proposed scaling (for different chain lengths) is indeed possible at high temperatures has been shown previously for the bond-fluctuation model (with a different energy function) in ref 28 and is also found in other simulations.[18,23] At low temperatures, however, the structure of the various profiles differs considerably from that at high temperatures so that the simple rescaling of the coordinate axes should not be expected to make the profile collapse. Nevertheless, we attempted such a scaling for $2R_{G\perp}^2(z)$, the profile which is least perturbed by the presence of the hard wall at low temperatures. The result is shown in Figure 17. As expected, the $2R_{G\perp}^2(z)$ profiles coincide at high temperatures (i.e., for $T \geq 0.6$). At these temperatures the bulk radius of gyration is the relevant large length scale which determines the temperature dependence of the profiles. This is no longer true for $T \leq 0.35$. Although the $2R_{G\perp}^2(z)$ profiles are again similar to each other, the increase of $R_{G\perp}$ with decreasing temperature is too weak to yield a successful scaling. However, a glance at Figure 5 suggests that ζ_m might be a better scaling variable. Therefore we attempted to plot $R_{G\perp}^2(z)/R_{G\perp}^2$ against z/ζ_m. The result is shown in Figure 18. In fact, $2R_{G\perp}^2(z)$ profiles for $T \leq 0.35$ now collapse fairly well onto a master curve which can be fitted by $R_{G\perp}^2(z)/R_{G\perp}^2 = 1 - \exp[-a(z/\zeta_m)^b]$ with $a = 0.75 \pm 0.05$ and $b = 1.85 \pm 0.30$. Since the temperature dependence of ζ_m for $T \geq 0.6$ is additionally comparable to that of $R_{G\perp}$, ζ_m is a suitable scaling variable over the whole temperature range (except at intermediate temperatures (i.e., $T = 0.35-0.6$), where the $2R_{G\perp}^2(z)$ profiles change shape) and thus the relevant length scale which characterizes the extent of the interphase in the glassy polymer melt under study.

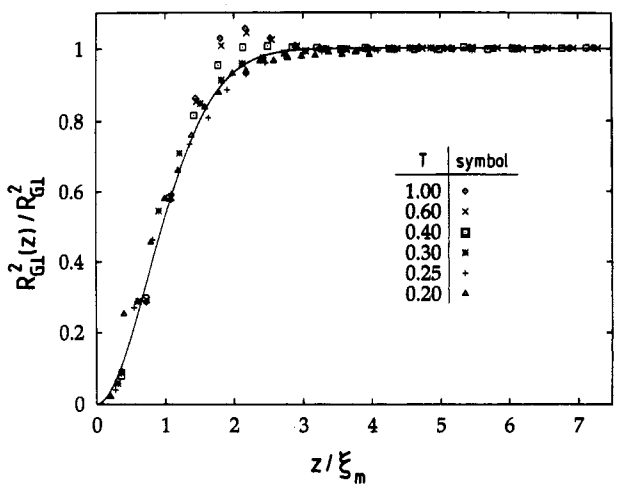

Figure 18. Plot of $R_{G\perp}{}^2(z)/(R_{G\perp}^{bulk})^2$ versus z/ζ_m for various representative temperatures: $T = 1.0$ (◇), $T = 0.6$ (×), $T = 0.4$ (□), $T = 0.3$ (*), and $T = 0.2$ (△). The z value of the profiles is that of the center of mass of the polymer.

IV. Summary and Outlook

Monte Carlo simulations are reported for the structural properties of a dense polymer melt confined between two hard walls. The polymer melt is simulated by the bond-fluctuation model on a simple cubic lattice. In addition to the excluded volume interaction an energy function is associated with long bond vectors, which makes the polymers expand and stiffen with decreasing temperatures. The competition between this energy function and the density causes a large increase of the structural relaxation time at low temperatures and generates the glassy behavior of the (unconfined) melt. In this simulation the temperature was varied from values typical of the ordinary liquid to those typical of the strongly supercooled melt. The interplay of temperature, packing effects, and wall constraints influences the structure of the polymer melt in the following way:

At high temperatures, when the contribution of the energy function is not yet very important, the structure of the polymers close to the wall is determined by the competition of the loss in configurational entropy due to the proximity of the impenetrable wall and the packing constraints exerted by the polymers further away in the bulk. This competition leads to an enhancement of the monomer and of the end-monomer density at the wall. The profiles of these monomer densities are oscillating functions which decay toward the bulk value on the length scale of a bond. Contrary to that, the density profile of the chains is enhanced at a distance comparable to the bulk value of the radius of gyration and strongly decreased in the immediate vicinity of the wall. The few chains lying in this vicinity are preferentially oriented parallel to the wall. Although the detailed shape of these profiles certainly reflects the underlying lattice structure, the general aspects of the profiles described above are also observed in many off-lattice simulations and are thus not a peculiarity of the lattice model employed.

When the melt is progressively supercooled the tendency of the polymers to align parallel to the wall becomes strongly reinforced by the influence of the energy function. Contrary to high temperatures the layer at the wall is no longer depleted of but enriched by almost two-dimensional polymer chains. These preferentially two-dimensional chain configurations persist over a distance of about twice the bulk value of the radius of gyration. However, larger distances are required for the chains to adopt the bulk behavior completely. At low temperatures the radius of gyration is thus not the largest length scale characterizing the extent of the interfacial region contrary to high temperatures.

The simulation results presented were concerned with the structural properties of the confined polymer melt only. Certainly, it is also interesting to study how energy, packing, and wall constraints influence the dynamic properties of this model. Work in this direction is in progress. In addition, the model studied hitherto ignores all kinds of attractive interactions among the monomers and between the monomers and the wall. That these attractive interactions might play an important role when one tries to compare theoretical and experimental results is discussed in ref 41, for instance. Therefore we plan to include these interactions in our model in the future.

Acknowledgment. We are very grateful to the Höchstleistungsrechenzentrum (HLRZ) at Jülich and to the Regionales Hochschulrechenzentrum Kaiserslautern (RHRK) for a generous grant of computer time on the CRAY-YMP and to Bundesministerium für Forschung und Technologie (BMFT; Grant Number 03M4076A3) for financial support. Special thanks go to Matthias Wolfgardt for assistance during implementation of the slithering snake algorithm and to Wolfgang Paul for several helpful discussions during various stages of this work.

References and Notes

(1) Newaz, G. M. In *Materials Science and Technology*; Chou, T.-W., Ed.; VCH: Weinheim, 1993; Vol. 13.
(2) Ishida, H.; Bussi, P. In *Materials Science and Technology*; Chou, T.-W., Ed. VCH: Weinheim, 1993; Vol. 13.
(3) Gandhi, M. V.; Thompson, B. S. *Smart Materials and Structures*; Chapman & Hall: London, 1992.
(4) Lovell, D. R. *Carbon and High-Performance Fibres Directory*; Chapman & Hall: London, 1991.
(5) Wolf, D., Yip, S., Eds. *Materials Interfaces: Atomic-level Structure and Properties*; Chapman & Hall: London, 1991.
(6) Flower, H. M. *High-Performance Materials in Aerospace*; Chapman & Hall: London, 1992.
(7) Doi, M.; Edwards, S. F. *Theory of Polymer Dynamics*; Clarendon Press: Oxford, U. K., 1986.
(8) Tirrell, M.; Parsonage, E. E. In *Materials Science and Technology*; Thomas, E. L., Ed. VCH: Weinheim, 1993; Vol. 12.
(9) Stamm, M. *Adv. Polym. Sci.* **1992**, *100*, 357.
(10) Factor, B. J.; Russell, T. P.; Toney, M. F. *Macromolecules* **1993**, *26*, 2847.
(11) Fleer, G. J.; Cohen Stuart, M. A.; Scheutjens, J. M. H. M.; Cosgrove, T.; Vincent, B. *Polymers at Interfaces*; Chapman & Hall: London, 1993.
(12) Sanchez, I. C., Ed. *Physics of Polymer Surfaces and Interfaces*; Butterworth-Heinemann: Boston, 1992.
(13) Yoon, D. Y.; Vacatello, M.; Smith, G. D. In *Monte Carlo and Molecular Dynamics Simulations in Polymer Science*; Binder, K., Eds.; Oxford University Press: New York (in press).
(14) Hariharan, A.; Harris, J. G. *J. Chem. Phys.* **1994**, *101*, 4156.
(15) Zhan, Y.; Mattice, W. L. *Macromolecules* **1994**, *27*, 7056.
(16) Chakraborty, A. K.; Adriani, P. M. *Macromolecules* **1992**, *25*, 2470; **1991**, *24*, 5226.
(17) Mansfield, K. F.; Theodorou, D. N. *Macromolecules* **1991**, *24*, 6283.
(18) Bitsanis, I. A.; Hadziioannou, G. *J. Chem. Phys.* **1990**, *92*, 3827.
(19) Lai, P.-Y. *Phys. Rev. E* **1994**, *49*, 5420.
(20) Vacatello, M. *Macromol. Theory Simul.* **1994**, *3*, 325.
(21) Vacatello, M. *Macromol. Theory Simul.* **1993**, *2*, 77.
(22) Vacatello, M.; Yoon, D. Y.; Laskowski, B. C. *J. Chem. Phys.* **1990**, *93*, 779.

(23) Kumar, S. K.; Vacatello, M.; Yoon, D. Y. *Macromolecules* **1990**, *23*, 2189.
(24) Kumar, S. K.; Vacatello, M.; Yoon, D. Y. *J. Chem. Phys.* **1988**, *89*, 5206.
(25) Bitsanis, I. A.; ten Brinke, G. *J. Chem. Phys.* **1993**, *99*, 3100.
(26) ten Brinke, G.; Ausserre, D.; Hadziioannou, G. *J. Chem. Phys.* **1988**, *89*, 4374.
(27) Pakula, T. *J. Chem. Phys.* **1991**, *95*, 4685.
(28) Wang, J.-S.; Binder, K. *J. Phys. I* **1991**, *1*, 1583.
(29) Dickman, R. *J. Chem. Phys.* **1992**, *96*, 1516.
(30) Dickman, R. *Comput. Polym. Sci.* **1991**, *1*, 206.
(31) Hertanto, A.; Dickman, R. *J. Chem. Phys.* **1990**, *93*, 774.
(32) Dickman, R.; Hall, C. K. *J. Chem. Phys.* **1988**, *89*, 3168.
(33) Wattenbarger, M. R.; Chan, H. S.; Evans, D. F.; Bloomfield, V. A.; Dill, K. A. *J. Chem. Phys.* **1990**, *93*, 8343.
(34) Yethiraj, A. *J. Chem. Phys.* **1994**, *101*, 2489.
(35) Yethiraj, A.; Hall, C. K. *Macromolecules* **1990**, *23*, 1865.
(36) Mansfield, K. F.; Theodorou, D. N. *Macromolecules* **1989**, *22*, 3143.
(37) Madden, W. G. *J. Chem. Phys.* **1988**, *89*, 3934; **1987**, *87*, 1405.
(38) Brazhnik, P. K.; Freed, K.; Tang, H. *J. Chem. Phys.* **1994**, *101*, 9143.
(39) Sen, S.; Cohen, J. M.; McCoy, J. D.; Curro, J. G. *J. Chem. Phys.* **1994**, *101*, 9010.
(40) Phan, S.; Kierlik, E.; Rosinberg, M. L.; Yethiraji, A.; Dickman, R. *J. Chem. Phys.* **1995**, *102*, 2141.
(41) Yethiraj, A.; Kumar, S.; Hariharan, A.; Schweizer, K. S. *J. Chem. Phys.* **1994**, *100*, 4691.
(42) Woodward, C. E.; Yethiraj, A. *J. Chem. Phys.* **1994**, *100*, 3181.
(43) Walley, K. P.; Schweizer, K. S.; Peanasky, J.; Cai, L.; Granick, S. *J. Chem. Phys.* **1994**, *100*, 3361.
(44) Kierlik, E.; Rosinberg, M. L. *J. Chem. Phys.* **1994**, *100*, 1716.
(45) Mayes, A. M. *Macromolecules* **1994**, *27*, 3114.
(46) Theodorou, D. N. *Macromolecules* **1988**, *21*, 1391; **1988**, *21*, 1400.
(47) de Gennes, P. G. *Adv. Colloid Interface Sci.* **1987**, *27*, 189.
(48) Jackson, C. L.; McKenna, G. B. *J. Non-Cryst. Solids* **1991**, *131–133*, 221.
(49) Schüller, J.; Mel'nichenko, Yu. B.; Richert, R.; Fischer, E. W. *Phys. Rev. Lett.* **1994**, *73*, 2224.
(50) Fehr, T.; Löwen, H. Glass transition in confined geometry (preprint).
(51) Keddie, J. L.; Jones, R. A. L.; Cory, R. A. *Europhys. Lett.* **1994**, *27*, 59.
(52) Keddie, J. L.; Jones, R. A. L. Glass Transition Behaviour in Ultra-Thin Polystyrene Films (preprint).
(53) Keddie, J. L.; Jones, R. A. L.; Cory, R. A. *Interface and Surface Effects on the Glass Transition Temperature Thin Polymer Films* (preprint).
(54) Wittmann, H.-W.; Kremer, K. *Comput. Phys. Commun.* **1992**, *71*, 343. Wittmann, H.-W.; Kremer, K. *Comput. Phys. Commun.* **1990**, 61, 309. Deutsch, H.-P.; Binder, K. *J. Chem. Phys.* **1991**, *94*, 2294. Carmesin, I.; K. Kremer, K. *Macromolecules* **1988**, *21*, 2819.
(55) Kremer, K.; Binder, K. *Comput. Phys. Rep.* **1988**, *7*, 259.
(56) Deutsch, H.-P.; Dickman, R. *J. Chem. Phys.* **1990**, *93*, 8983.
(57) Baschnagel, J.; Binder, K. *Physica A* **1994**, *204*, 47.
(58) Paul, W.; Baschnagel, J. In *Monte Carlo and Molecular Dynamics Simulations in Polymer Science*; Binder, K., Ed.; Oxford University Press: New York (in press).
(59) Wolfgardt, M.; Baschnagel, J.; Binder, K. *J. Chem. Phys.*, in press.
(60) Rössler, E.; Sillescu, H. In *Materials Science and Technology*; Zarzycki, J., Ed.; VCH: Weinheim, 1991; Vol. 10.
(61) McKenna, G. B. In *Comprehensive Polymer Science*; Booth, C., Price, C., Eds.; Pergamon Press: NY, 1989; Vol. 2.
(62) Paul, W.; Binder, K.; Heermann, D. W.; Kremer, K. *J. Phys. II* **1991**, *1*, 37.
(63) Sokal, A. D. In *Monte Carlo and Molecular Dynamics Simulations in Polymer Science*; Binder, K., Ed.; Oxford University Press: New York (in press).
(64) Temperature is measured in units of ϵ/k_B, where ϵ is the parameter of the bond vector energy (see text and ref 57 for further explanations). All length and time scales are measured in units of lattice constants and of Monte Carlo steps, respectively.
(65) Wolfgardt, M.; Baschnagel, J.; Binder, K. *J. Phys. II Fr.* **1995**, *5*, 1035.

MA9505080